Annals of Biomedical Engineering (© 2020)
https://doi.org/10.1007/s10439-020-02524-x

BMES BIOMEDICAL ENGINEERING SOCIETY

Original Article

Electro-Thermal Therapy Algorithms and Active Internal Electrode Cooling Reduce Thermal Injury in High Frequency Pulsed Electric Field Cancer Therapies

MICHAEL B. SANO, CHRISTOPHER C. FESMIRE, and ROSS A. PETRELLA

UNC – NCSU Joint Department of Biomedical Engineering, Raleigh, NC, USA

(*Received 30 August 2019; accepted 27 April 2020*)

Associate Editor Agata A. Exner oversaw the review of this article.

Abstract—Thermal tissue injury is an unintended consequence in current irreversible electroporation treatments due to the induction of Joule heating during the delivery of high voltage pulsed electric fields. In this study active temperature control measures including internal electrode cooling and dynamic energy delivery were investigated as a process for mitigating thermal injury during treatment. *Ex vivo* liver was used to examine the extent of thermal injury induced by 5000 V treatments with delivery rates up to five times faster than current clinical practice. Active internal cooling of the electrode resulted in a 36% decrease in peak temperature vs. non-cooled control treatments. A temperature based feedback algorithm (electro-thermal therapy) was demonstrated as capable of maintaining steady state tissue temperatures between 30 and 80 °C with and without internal electrode cooling. Thermal injury volumes of 2.6 cm^3 were observed for protocols with 60 °C temperature set points and electrode cooling. This volume reduced to 1.5 and 0.1 cm^3 for equivalent treatments with 50 °C and 40 °C set points. Finally, it was demonstrated that the addition of internal electrode cooling and active temperature control algorithms reduced ETT treatment times by 84% (from 343 to 54 s) vs. non-cooled temperature control strategies with equivalent thermal injury volumes.

Keywords—Electro-thermal therapy, Focal ablation, Non-thermal irreversible electroporation, H-FIRE, Liver cancer.

INTRODUCTION

Surgically inoperable tumors which form near major blood vessels or critical structures (e.g. hepatic veins, inferior vena cava, and biliary tract) are currently being treated using irreversible electroporation (IRE).[30] IRE has been indicated for these treatments due in part to being recognized as a non-thermal therapy.[11,13] However, this designation is explicitly related to the mechanism of cell death (rupture of the cell membrane caused by high voltage pulsed electric fields[40]) and not the absence of tissue heating during treatment.[7]

In practice, IRE treatments must be completed under the time restraints of general anesthesia,[24] requiring pulses to be delivered in a relatively short period of time which results in measurable tissue heating.[7] For example, *in vivo* porcine experiments demonstrate that 70–100 μs, 1 Hz pulses delivered by the NanoKnife system[18] (NK-IRE, AngioDynamics, Latham, NY) have the ability to rapidly induce Joule heating to the point of tissue coagulation.[7] Without consideration of local temperature profiles, heating may contribute to rare, but documented, adverse side effects of NK-IRE including coagulative necrosis,[7] thrombosis,[27] abscesses,[30] and fistulas.[21] Nevertheless, promising early clinical trials indicate a significant utility for NK-IRE as a treatment of inoperable tumors[22,23,33] while the need for temperature control in NK-IRE has been recognized.[31] To address the effects of Joule heating, several electrode design modifications have previously been proposed. Irrigation of chilled solutions directly into the tissue during NK-IRE treatments has been demonstrated.[38] Electrodes filled with a phase change material which absorbs thermal energy at or below temperatures associated with thermal injury have also been proposed.[2] Additionally, internally liquid cooled electrodes similar to that used in microwave ablation[19,20] have also been examined.[31,38]

Address correspondence to Michael B. Sano, UNC – NCSU Joint Department of Biomedical Engineering, Raleigh, NC, USA. Electronic mail: mikesano@med.unc.edu

Published online: 15 May 2020

These electrode cooling techniques have been successful approaches to mitigating the deleterious thermal effects associated with NK-IRE (e.g. electrical arcing), but a question of thermal dosing remains. There is some evidence which suggests that mild heating may be synergistic with pulsed electric fields[6] and treatments employing microsecond duration electrical pulses exhibit a significant positive temperature dependence.[9] Yet, the temperature increase should be controlled to avoid adverse side effects. Clinically the aim is to maximize pulse delivery rates to minimize treatment times, while maintaining a physician prescribed level of tissue heating. To execute this requires finding a steady state pulse protocol which is a function of applied voltage, pulse width, pulse number, delivery rate, tissue type, tumor position within the organ, unique tumor vascularization, and blood perfusion. To account for all of these variables *in situ* without the need for comprehensive computational electromagnetic pre-treatment planning, a treatment paradigm which dynamically adjust the pulse parameters to the tissue conditions has been conceived.

Electro-thermal therapy (ETT) describes a pulsed electric field (PEF) treatment in which the pulse delivery rate is dynamically changed in order to regulate local tissue temperature. ETT utilizes a system controls approach, using temperature as process feedback to manage the intra-tumor environment. Preliminary studies have validated that this technique is capable of achieving and maintaining steady state temperatures while delivering a specified dose using *in vitro* models.[32] These studies indicate that integration of temperature feedback control typically necessitates an increase in treatment duration. This is due to the need to deliver a specified electrical dose (integrated time) to achieve the prescribed ablation volume[34,36] while the energy delivery rates are dynamically reduced to constrain tissue heating. While moderate increases in treatment time may be acceptable in certain scenarios, there is a need for ablative techniques which simultaneously prevent thermal injury while minimizing overall treatment durations.

An emerging characteristic of PEF treatments employing microsecond duration electrical pulses is that the rate of energy delivery plays a relatively small role in the ablative outcomes.[36] Instead, the applied voltage,[17] tissue temperature,[9] and total dose[34,36] act as the primary drivers for ablation size. These key characteristics enable the use of techniques which maximize energy delivery rates to minimize treatment times.

For the first time this study demonstrates the feasibility of active cooling via an internally perfused electrode combined with ETT algorithmic control of *in situ* temperature profiles for tissue ablation. This was evaluated in an *ex vivo* tissue model with a single internally cooled applicator and grounding pad (CA + GP). A fiberoptic temperature sensor placed at either the tissue-electrode or tissue-insulator interface was used to acquire temperature feedback data and demonstrate the feasibility of this approach. The electrode configuration was used to deliver 5000 V treatments to tissue with pulse delivery rates up to 500 μs/s. The treatments were evaluated for temperature profiles, pulse delivery rates, time to completion, and extent of thermal injury. Actively cooled ETT treatments were then compared to non-cooled treatments. Numerical simulations were then used to predict the ratio of thermal damage to electrical ablation volume based on existing experimental data.

The results of this analysis indicate that active cooling of the applicator reduced thermal injury volumes by 56–84% vs. non-cooled treatments. While actively cooling the electrodes, the largest thermal injury volumes (2.6 ± 0.4 cm^3) were observed for treatments with a 60 °C temperature set point. Reduction of this set point to 50 °C and 40 °C resulted in significantly smaller thermal injury volumes of 1.5 ± 0.3 and 0.1 ± 0.2 cm^3, respectively, without significantly increasing treatment times. A combination of active cooling and temperature control (2.0 mL/min, 40 °C) was found to reduce treatment times by 84% (from 5.4 to 0.9 min) without significantly increasing the extent of thermal injury found for matched non-cooled ETT treatments. These results confirm the use of active electrode cooling combined with ETT is a viable strategy for reducing thermal injury in pulsed electric field therapies and sets the foundation for *in vivo* studies.

MATERIALS AND METHODS

A modified 1.44 mm diameter internally cooled applicator (Cool-Tip RF ACT1520, Medtronic Inc., Minneapolis, Minnesota) with a 2 cm electrode exposure was used to administer the treatments. To equip the electrode for high voltage experiments, the applicator handle was removed and the electrical leads form the internal temperature sensor were clipped to prevent a short circuit through the component. The original low voltage electrical lead was replaced with 10 kV rated silicone coated wire (6733-2, Pomona Electronics Inc., Everett, WA) and exposed metal at the proximal end was wrapped in polyimide and shrink wrap tubing. A fiberoptic temperature sensor (TS5, Micronor Inc., Camarillo, CA) was affixed to each applicator such that the temperature sensing element was approximately half way in the exposed area or 1 cm from the distal tip of the electrode (Fig. 1a) or at the electrode-

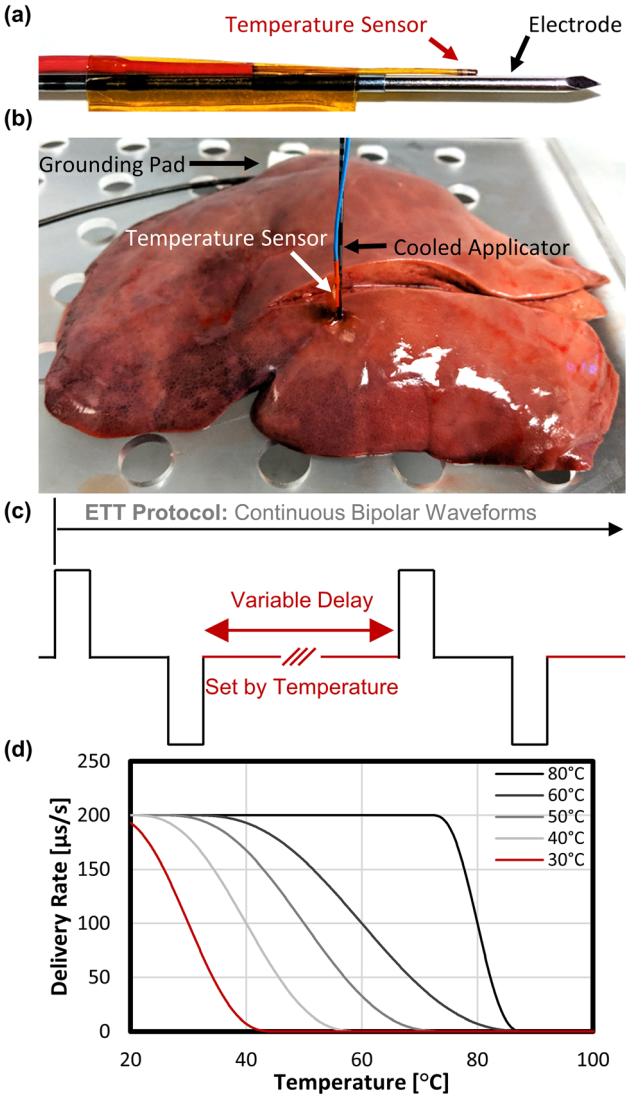

FIGURE 1. Overview of ETT treatment protocol. (a) A fiber optic temperature sensor was attached to an internally cooled applicator with a 2 cm exposed electrode. (b) The assembly was inserted into *ex vivo* tissue such that the entire applicator and 5 mm of insulation were below the tissue surface and energy was delivered via the electrode and a distal grounding pad (A + GP). (c) A 2-5-2 waveform was repeated continuously with a variable delay determined by the (d) temperature dependent control algorithm to achieve a desired energy delivery rate. Treatment continued until a specified integrated energized time (dose) was achieved.

insulator interface (Supplemental Fig. 1a). In all experiments, the applicator was placed vertically into the tissue such that the entire electrode and an additional 5 mm of insulator were beneath the tissue surface (Fig. 1b). A 4 × 5 cm aluminum foil grounding pad was placed underneath the tissue served as the return path to the pulse generator.

Electrical pulses with amplitudes of 5000 V were delivered using a custom pulse generator based on an H-Bridge topology which included a 100 MSPS data acquisition system to record voltage and current waveforms in real time (Supplemental Fig. 2). Temperatures were acquired by a signal conditioner (Fotemp, Micronor Inc., Camarillo, CA). Data was transmitted over USB and recorded at 3 Hz by a custom Python application which controlled the pulse generation system.

All experiments were conducted using a waveform consisting of a 2 μs positive polarity pulse, a 5 μs delay, and a 2 μs negative polarity pulse (2-5-2 waveform, Fig. 1c). This waveform was repeated to deliver a specified electrical dose with an integrated energized time (IET) calculated as:

$$\mathrm{IET} = \sum_{0}^{N} (\tau_p + \tau_n)[\mathrm{s}] \tag{1}$$

where N is the total number of waveforms delivered and τ_p and τ_n are the positive and negative pulse durations (2 μs), respectively. The total time required to deliver the target IET (0.01 s or 0.02 s) was automatically recorded and values are reported here as mean ± standard deviation.

The delay (δ) between sequential 2-5-2 waveforms was either held constant or dynamically adjusted using a temperature control algorithm to achieve a specified pulse delivery rate (R) calculated as:

$$R = \frac{\tau_p + \tau_n}{\delta}[\mu\mathrm{s/s}] \tag{2}$$

When enabled, the temperature control algorithm determined the rate (R) at which waveforms were delivered:

$$R(T) = R_{\max} \cdot \rho(T)[\mu\mathrm{s/s}] \tag{3}$$

$$\rho(T) = 0.5 - 0.9375 \cdot \Gamma(T) + 0.625 \cdot \Gamma(T)^3 - 0.1875 \cdot \Gamma(T)^5 \tag{4}$$

$$\Gamma(T) = \frac{T - T_t}{\beta} \tag{5}$$

$$\beta = T_t \times \omega \tag{6}$$

where $R_{\max}$ is the maximum pulse delivery rate [μs/s] prescribed, T is the instantaneous temperature [°C], T_t is the target temperature [°C], and ω is a coefficient affecting the slope between maximum and minimum energy delivery rates. After preliminary calibration experiments (Supplemental Fig. 1b) this was held constant at 0.5 for all experiments except those with an 80 °C set point which required a more aggressive energy delivery profile (ω = 0.1) to reach the target temperature (Fig. 1d). This metric of pulse delivery

rate with units of μs/s was used to enable comparison to protocols which utilize longer[31] (e.g. 50–100 μs) and shorter[17] (e.g. 0.5–2.0 μs) pulses with approximately equivalent average power, but different pulse repetition rates. The treatment temperature profiles are presented as the mean ± standard deviation when R was held constant. For temperature controlled treatments the median length treatment is presented due to variation in treatment lengths producing non-representative mean temperature profiles.

Active cooling of the applicator was accomplished via perfusion with ice water which was circulated using a peristaltic pump (EW-77921-65, Cole-Palmer, Vernon Hills, IL) attached to the applicators fluid input tubing. In all actively cooled experiments, fluid flow (1–8 mL/min) was started prior to placement of the applicator and treatments were initiated as soon as safely possible after insertion of the applicator into the tissue to avoid substantially pre-cooling the treatment site.

Numerical Simulation of ETT and Thermal Ablation Volumes

It was of interest to investigate the potential relative volumes of both ETT and Thermal ablation zones produced by the experimental treatments and to compare these to comparable RFA treatments. Time domain 2D axisymmetric finite element simulations incorporating electrodynamics, thermodynamics, and fluid dynamics components were created using COMSOL Multiphysics (Version 5.3, COMSOL Inc., Los Altos, CA) following previously defined methods[17,34,35] with the addition of a thermal damage model[8,12,37] (see Supplemental Materials). ETT ablation volumes were determined based on lethal electric field thresholds determined in *ex vivo* liver for treatments with IET of 0.01–0.04 s.[17] To approximate ETT ablation growth as a function of applied dose, a piecewise cubic function (Supplemental Fig. 3) was used to map the instantaneous IET to a lethal threshold between 6400 V/cm (0.001 s IET) and 587 V/cm (0.04sIET). A parametric conductivity sweep was conducted to match the simulated current to experimental values.

The internal geometry of the cooled applicator was approximated as a 0.51 mm diameter tube (Supplemental Fig. 3b) inside of the 1.44 mm diameter electrode applicator. Two rounds of adaptive meshing were implemented using the electric field as an error indicator (Supplemental Fig. 3c, d) to ensure convergence. The final mesh contained 839,941 elements and required approximately 2–3 h to solve 400 s time domain simulations on a ten core Intel i7-6950X CPU with 64 GB of RAM.

Effect of Coolant Flow Rate on Thermal Injury

It was of interest to determine how treatment parameters affected thermal injury at the electrode-tissue interface. *Ex vivo* liver tissue was used to assess the induction of thermal injury in a clinically relevant organ. To maximize the potential of inducing thermal injury, 0.02 s IET 5 kV treatments were administered with an R_{max} of 500 μs/s. This IET (0.02 s) is approximately the dose prescribed for clinical NK-IRE treatments (e.g. 90 × –220 ×, 70–100 μs pulses, 0.006–0.022 IET) and is typical for high frequency IRE treatments.[17]

Fluid flow rates of 0.0 (no cooling), 1.0, 2.0, 4.0, and 8.0 mL/min were investigated. To prevent extreme temperatures which can result in tissue desiccation, arcing, and damage to the pulse generator, these experiments were conducted with a temperature set point of 80 °C. To mitigate the impact of treatment current as a confounding factor, the grounding pad was moved to obtain consistent mean currents, measured throughout the treatment (range: 18.3–21.1 A) for these protocols. To achieve this, a single test waveform was delivered and the grounding pad was moved accordingly to adjust the initial current to approximately 18 A.

Effect of Temperature Set Point on Thermal Injury

To investigate the effect of ETT temperature set point on thermal injury 0.02 s IET 5000 V treatments were administered with an R_{max} of 500 μs/s and a perfusion flow rate of 2.0 mL/min with temperature set points of 40, 50, and 60 °C. In some actively cooled temperature controlled treatments the measured temperature failed to reach the 40, 50, or 60 °C target set points. This may have been due to deflection of the temperature sensor away from the electrode-tissue interface or elevated tissue impedance. These treatments were excluded from analysis and additional data points were acquired.

Treatments comparing the ETT waveforms to those used by the clinical NK-IRE protocols were attempted, however, intense electrical arcing was observed for 100 μs monopolar waveforms in preliminary experiments at 4000 V (Supplemental Fig. 4, Supplemental Video 1) and these treatments were aborted to avoid damaging the pulse generator. All other protocols were repeated a minimum of three times (N = 3). A full accounting of the experimental parameters investigated in this study is presented in Table 1.

Following treatment, the liver tissue was sectioned along the applicator insertion path. Some treatment locations contained a distinctly lighter region of tissue with a porous texture consistent with thermal injury.[3]

TABLE 1. Summary of experimental conditions investigated.

Experimental voltage [V]	Cooling rate [mL/min]	Temperature set point [°C]	Replicates	Thermal volume [cm^3]	Treatment time [s]
5000	–	80	4	0.8 ± 0.2	68.3 ± 1.0
Fig. 3	1	80	3	1.2 ± 0.4	40.8 ± 0.0
	2	80	3	0.2 ± 0.2	40.8 ± 0.0
	4	80	3	0.4 ± 0.1	40.8 ± 0.0
	8	80	3	0.1 ± 0.1	40.7 ± 0.0
5000	–	50	8	0.3 ± 0.3	342.9 ± 220.5
Fig. 4	2	40	5	0.1 ± 0.2	53.7 ± 16.7
	2	50	3	1.5 ± 0.3	48.3 ± 5.3
	2	60	3	2.6 ± 0.4	43.1 ± 4.0

Dash symbols (–) indicate non-cooled experiments.

The treatment sites were photographed and measurements of the maximal width (w, perpendicular to the applicator) and maximal length (l, parallel to the applicator) of the thermal injury zone was measured for each side of the tissue section. The volume of thermal injury was then calculated as:

$$V = \frac{\pi}{6} l \cdot w^2 \left[\text{cm}^3\right] \quad (7)$$

Treatment sites where the needle path could not be identified due to improper sectioning were excluded from evaluation to avoid under estimating the extent of thermal injury present. Values for each treatment parameter were then averaged and are presented here as mean ± standard deviation. Statistical analysis was completed via a one sided Student's T Test assuming unequal variances and an alpha level of 0.05 using JMP Pro 14 (SAS Institute Inc., Cary, NC).

RESULTS

Numerical Predictions of ETT and Thermal Ablation Sizes

Experimental current observations indicated a tissue impedance of approximately 273 Ω between the electrode and grounding pad. A preliminary parametric analysis of the simulated tissue domain yielded a matching electrical conductivity of 0.11 S/m for the liver tissue which is in agreement with literature values reported at 500 kHz.[10] Simulations predicting the extent of thermal injury following 100% duty cycle RFA treatments with amplitudes of 25 V and 50 V indicated thermal injury volumes of 0.0 and 0.6 cm^3, respectively, following a 100 s treatment (Fig. 2a and b). As the electric field in these RFA treatments was not sufficient to induce electroporative effects, 0.0 cm^3 ETT ablation volumes were predicted for these treatments.

Simulated 5000 V 0.02 s ETT treatments without cooling resulted in a predicted thermal injury volume of 2.1 cm^3 when energy was delivered at a rate of 200 μs/s. Induction of internal electrode cooling with fluid flow rates of 1, 2, 4, and 8 mL/min reduced these predicted thermal injury volumes to 1.5, 1.0, 0.5, and 0.1 cm^3, respectively. In each ETT simulation, the tissue received a dose of 0.02 s resulting in a predicted ETT ablation volume of 12.5 cm^3.

Numerical simulations at experimental flow rates (Fig. 2c, d and Supplemental Fig. 5a–c) indicate that

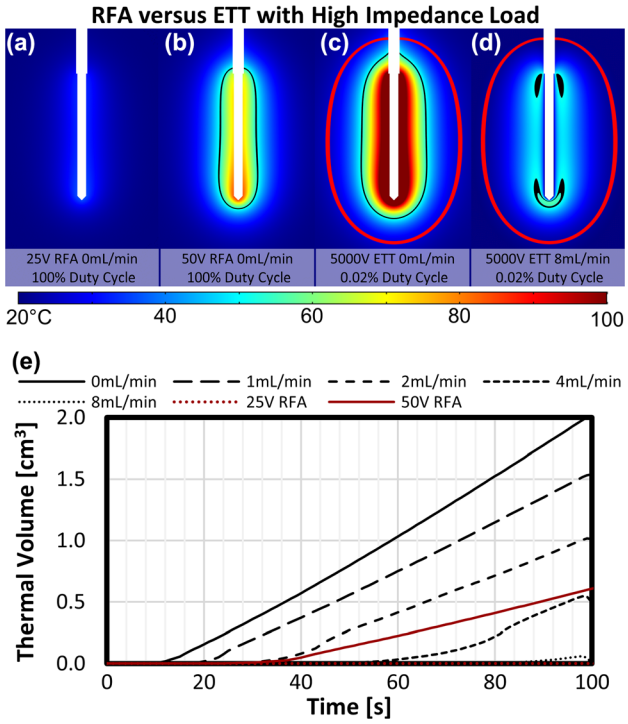

FIGURE 2. Simulated thermal damage (black contours) and ETT ablation volumes (red contours) following a 100 s treatment with RFA or ETT. RFA simulations were conducted with either 25 V or 50 V delivered with a 100% duty cycle without cooling. 5000 V 0.02 s ETT treatments were simulated with a 0.02% duty cycle (200 μs/s) and coolant flow rates of 0, 1, 2, 4, or 8 mL/min. ETT ablation volumes were calculated with an electric field threshold of 690 V/cm consistent with a dose of 0.02 s.

internal electrode cooling reduces the maximum temperature at the electrode-tissue interface as well as the peak temperature within the tissue. When cooling is implemented, the location of maximum temperature shifts from the electrode-tissue interface outward into the tissue (Supplemental Fig. 5d). Similarly, the transient rate of temperature increase (Supplemental Fig. 5e) decreases as the coolant flow rate increases. This reduces the predicted thermal injury volume (Fig. 2e and Supplemental Fig. 5f), but not the predicted ETT ablation volume (Supplemental Fig. 5 g).

Similar results were found for simulations conducted with energy delivery rates of 500 μs/s (Supplemental Fig. 6) which indicated that coolant flow rates of 8 mL/min or greater would be required to constrain peak tissue temperatures to below 100 °C. In these simulations, implementation of temperature control (Supplemental Fig. 7) reduced the predicted thermal injury volume at the expense of increasing predicted treatment times. Simulations implementing a temperature set point of 40 °C with active cooling at 2 mL/min resulted in a similar thermal injury volume (0.5 cm^3) compared to 50 °C simulations without active cooling (0.7 cm^3) while significantly reducing the predicted treatment duration (184 s vs 530 s). As each simulation delivered an equivalent dose (0.02 s), the predicted ETT ablation volume remained the same at 12.5 cm^3.

Validation of ETT Protocol and Active Cooling

Initial validation of the ETT protocol was conducted with the temperature sensor at the electrode-insulator interface (Supplemental Fig. 1a). 5000 V 0.02 s treatments were administered with an initial energy delivery rate of 200 μs/s. Without temperature control or active cooling the measured temperature transient logarithmically approached 60 °C (Supplemental Fig. 1b) over the course of the 100 s treatment. Some deviation from a consistent temperature profile was observed as the maximum temperature was approached indicating that temperatures in proximity to 100 °C may have been reached along the electrode.

Implementation of the temperature control with a 50 °C set point resulted in longer treatments (103–160 s) and temperature measurements which approached, but generally did not exceed the programmed temperature (Supplemental Fig. 1b). Selection of the parameter ω, which controls the slope of the control algorithm, had a minimal effect on the algorithm's performance. Selection of a value of 0.25 resulted in the fastest average treatments (110.0 ± 5.5 s) with increasing values of ω resulting in incrementally longer treatments of 134.0 ± 6.0 s (ω = 0.5), 140.0 ± 7.9 s (ω = 0.75), and 146.7 ± 11.8 s (ω = 0.99). Pervious experiments validating this technique *in vitro*[32] yielded a reduction in oscillations and an increase in stability when for larger values of ω and a value of 0.5 was utilized for the majority of the remaining experiments unless otherwise noted.

Effect of Coolant Flow Rate on Thermal Injury

A temperature sensor paced at the tissue-electrode interface, corresponding with the middle of the exposed region (Fig. 1a), was used to assess temperatures where the approximate peak temperatures would occur. Preliminary 5000 V 0.01 s IET treatments utilizing a fixed pulse delivery rate of 100 μs/s without cooling resulted in a mean temperature increase of 57.0 ± 10.9°C during the 100.0 ± 0.002 s duration treatments (Supplemental Fig. 8). These treatments reached peak temperatures of 78.8 ± 12.3 °C without approaching a steady state equilibrium. Dynamic energy delivery with temperature control was therefore implemented for all subsequent 5 kV treatments to prevent the tissue from reaching temperatures associated with tissue desiccation (approximately 100 °C) in the longer 0.02 s IET treatments evaluated.

Without cooling (0 mL/min), 5000 V ETT treatments with an R_{max} of 500 μs/s reached the 80 °C temperature set point in 33.0 ± 0.7 s (Fig. 3a) and maintained a temperature of 80.2 ± 0.4 °C for the duration of the treatment. These treatments had mean initial currents of 18.1 ± 0.4 A which increased to 21.5 ± 0.5 A (Fig. 3b). Following treatment, distinct zones of lighter tissue with a spongy texture, indicative of thermal injury[3,7,31] (Fig. 3c), were observed adjacent to the electrode insertion path (Fig. 3d). For the non-cooled treatments, these regions measured 0.83 ± 0.16 cm^3. Active cooling with perfusion rates of 1 mL/min, 2 mL/min, 4 mL/min, and 8 mL/min resulted in temperature profiles which failed to reach the 80 °C set point or a steady state before the 0.02 s IET treatment was completed. These treatments reached peak temperatures of 46.1 ± 2.2 °C, 35.3 ± 4.4 °C, 36.9 ± 4.6 °C, and 39.6 ± 3.1 °C, respectively (Fig. 3a). The 1 mL/min treatments resulted in the highest final currents of 22.3 ± 2.1 A, while the 8 mL/min treatments resulted in the lowest final currents of 19.1 ± 0.7 A with the 2 and 4 mL/min currents falling non-sequentially between these values (Fig. 3b). The largest thermal injury zones were found for the 1 mL/min treatment groups measuring 1.19 ± 0.40 cm^3 (Fig. 3c and e). These were found to be statistically significantly larger than the non-cooled (p = 0.004) and the remaining actively cooled treatments (p < 0.001) which measured 0.24 ± 0.17 cm^3, 0.37 ± 0.10 cm^3, and 0.13 ± 0.09 cm^3 for the 2

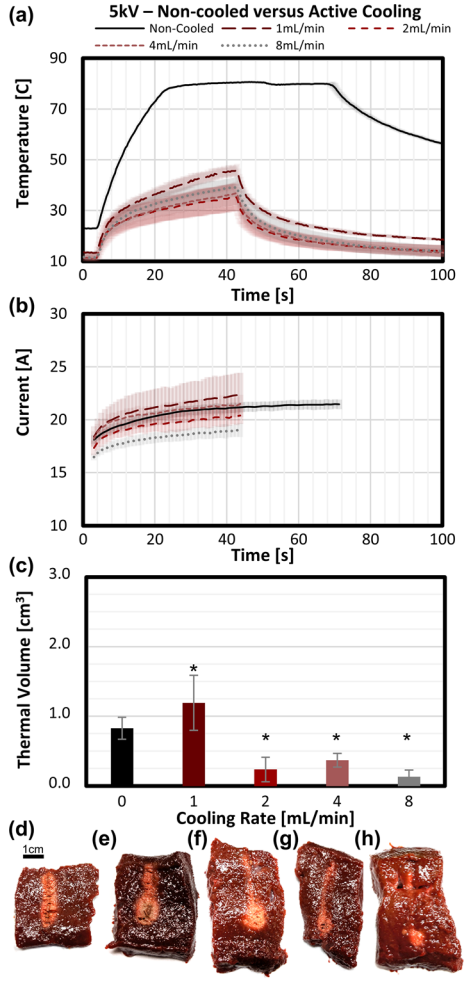

FIGURE 3. Thermal damage as a function of coolant perfusion rate. (a) Temperature and (b) current profiles for treatments with non cooled (0 mL/min), and active cooling with perfusion rates of 1, 2, 4, and 8 mL/min. (c) Calculated thermal damage volumes and representative gross sections from treatments with (d) 0, (e) 1.0, (f) 2.0, (g) 4.0, and (h) 8 mL/min cooling rates. * Indicates statistically significantly different than the non-cooled (0 mL/m) treatment group.

(Fig. 3f), 4 (Fig. 3g), and 8 mL/min (Fig. 3h) treatment groups, respectively. As the cooling rate increased, the thermal injury zone was observed to narrow along the electrode insertion path resulting in a teardrop shaped zone with the widest point occurring at the locations approximately corresponding to the electrode tip. While the 8 mL/min treatment group resulted in the smallest thermal injury zones, this group was not found to be statistically significantly different than the 2 mL/min ($p = 0.41$) or 4 mL/min ($p = 0.081$) treatment groups.

Effect of Temperature Set Point on Thermal Injury

To achieve temperature set points of 40, 50, and 60 °C (Fig. 4a) with active cooling, it was necessary to

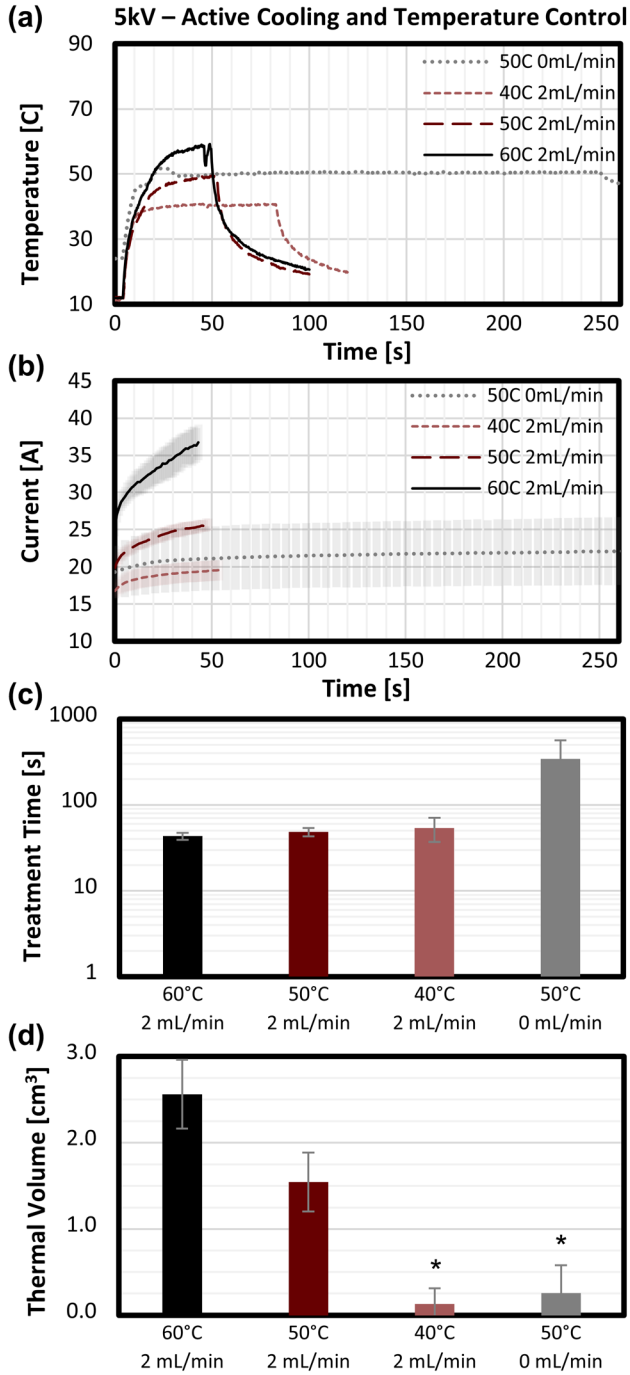

FIGURE 4. Thermal injury as a function of temperature set point with a fixed coolant perfusion rate of 2 mL/min. (a) Representative temperature plots for the median duration treatments for protocols with temperature set points of 40 °C, 50 °C and 60 °C. Treatments with passive cooling (0 mL/min) are additionally presented for 40 °C and 50 °C temperature set points. (b) Mean current as a function of time from t = 0 to the duration of the shortest treatment in each group. Shaded regions represent one standard deviation from the mean. (c) Mean treatment times and (d) thermal injury volumes for each treatment group.

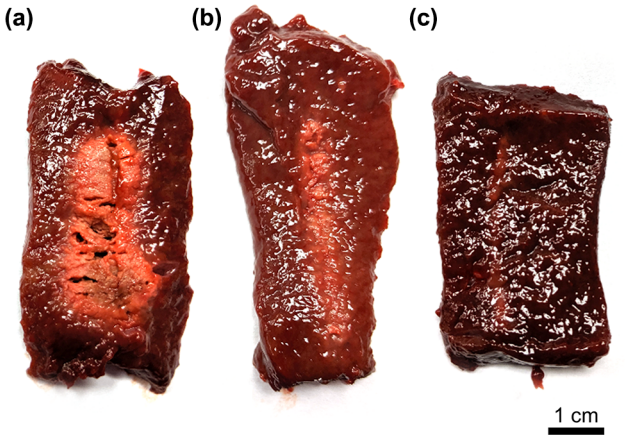

FIGURE 5. Representative cross sections from 5000 V ETT treatments cooled at a rate of 2 mL/min with temperature set points of (a) 60 °C, (b) 50 °C, and (c) 40 °C.

modify the distance between the electrode and grounding pad to achieve higher initial treatment currents (Fig. 4b) of 16.8 ± 1.1, 19.9 ± 0.8, and 25.0 ± 0.9 A, respectively. These treatments reached maximum currents of 19.8 ± 1.5, 25.8 ± 1.0, and 37.2 ± 3.1 A. The initial and maximum currents for non-cooled treatments with a set point of 50 °C measured 19.3 ± 3.5 and 22.4 ± 4.7 A, respectively. Actively cooled treatments with set points of 40, 50, and 60 °C required 53.7 ± 16.7, 48.3 ± 5.3, and 43.1 ± 4.0 s to complete, respectively (Fig. 4c). Non-cooled treatments with a temperature set point of 50 °C took significantly ($p < 0.011$) longer to complete (342.9 ± 220.5 s).

The largest thermal injury zones were observed for the actively cooled 60 °C temperature set point measuring 2.6 ± 0.4 cm^3 (Fig. 5a). Significantly ($p < 0.0001$) smaller thermal injury zones were observed for actively cooled treatments with 50 °C (1.5 ± 0.3 cm^3, Fig. 5b) and 40 °C (0.1 ± 0.2 cm^3, Fig. 5c) set points as well as the non-cooled 50 °C treatments which measured 0.3 ± 0.3 cm^3. There was not a significant difference between the thermal injury zones for the actively cooled 40 °C and non-cooled 50 °C treatments ($p = 0.35$).

DISCUSSION

Active cooling strategies are routinely implemented in radiofrequency[4,28] and microwave ablation[1,16] procedures with irrigating[29] or internally perfused[25,39] applicators. In RFA, these techniques are implemented to reduce charring at the electrode-tissue interface which limits ablation volumes.[14] Similarly, cooled microwave ablation applicators mitigate deleterious electrode heating due to poor impedance matching between the tissue and antenna which can cause off target heating adjacent to the applicator.[39] These strategies enable rapid the production of 3 cm (RFA, 12 min, 40 W)[14] to 5 cm (MWA, 10 min, 80 W)[39] spherical thermal lesions. In this study, baseline 5000 V treatments had an initial time-average power of approximately 45 W (500 μs/s 5000 V 18 A). Without active cooling these treatments (68 s average) produced a mean thermal injury zone measuring 2.9 × 0.7 cm, despite the regulation of an 80 °C maximum temperature. This is generally an unwanted effect in IRE procedures where avoiding thermal injury to critical adjacent structures is often the rationalization for selecting the treatment modality. Currently this is avoided by either reducing the electrode exposure to reduce treatment currents or by reducing the energy delivery rate to reduce the average power dissipated in the tissue.

This study examined two alternative techniques and their combination for mitigating thermal injury during IRE treatments: active cooling and computational control of pulse delivery. Active cooling in the absence of computational control algorithms was capable of reducing the peak temperature reached by 5000 V treatments by 51% vs. non-cooled treatments (with an 80 °C maximum enforced). Similar studies delivering 2700 V 300 × 100 μs pulses (0.03 s IET, 150 μs/s) in a perfused organ model observed a 22% decrease temperature rise when cooling with room temperature water at a perfusion rate of 35 mL/min.[31] The larger reduction of temperature observed in the present study may be accounted for in the use of near freezing coolant despite the elevated voltage and elevated pulse delivery rates. It should be noted that a smaller IET (0.02 s) was used in the present study and a less substantial temperature difference may be observed for longer treatments if a steady state equilibrium is reached in non-cooled treatments.

The combination of active cooling and temperature control enabled the delivery of a 0.02 s IET 5000 V treatment, greater in both dose and voltage than those currently administer clinically, in approximately 50–120 s with prescribed temperature increases of 10 °C, 20 °C, 30 °C, or 40 °C. Assuming an equivalent temperature rise is observed *in vivo*, this would correspond to a temperature set points of 47–87 °C. Temperatures in the range of 42–47 °C have been shown to induce thermal injury for exposure times on the order of hours while those above in the rage of 50–90 °C are generally considered to induce thermal injury for exposure times of minutes to seconds.[5,26] Manual strategies for mitigating thermal injury exist, including careful selection of pulse amplitudes, electrode exposures, and repetition timing. However, these techniques require *a priori* knowledge of a number of *in situ* biological charac-

teristics. These factors are unlikely to be taken into account in the existing clinical workflow which currently involves real-time treatment planning following electrode placement. Given these constraints, active temperature control in conjunction with electrode cooling may help simplify the clinical workflow while providing an additional means for reducing the risk of deleterious thermal damage.

The temperature at the electrode-tissue interface in actively cooled experiments was observed to decrease rapidly in the first few seconds after insertion. Most actively cooled experiments were conducted with an initial temperature between 9 and 14 °C which was 8–13 °C below baseline. While not ideal, the delay in initiating treatments was required to ensure that personnel were at a safe distance from the experimental setup. Accounting for the decreased baseline temperature active cooling resulted in a 38% reduction in temperature change vs. non-cooled 5 kV treatments. The use of low temperature coolants may enable pre-cooling of the tissue yielding additional protection against thermal injury. Future optimization will be necessary to determine optimal cooling times, coolant temperatures, and clinically acceptable minimum tissue temperatures.

It was found that the induction of thermal injury is not exclusively a function of temperature at the electrode-tissue interface. Preliminary experiments indicated that when treatments had identical temperature profiles (Supplemental Fig. 9a) and coolant perfusion rates (8 mL/min) the extent of thermal injury was instead dependent on the delivered electrical current (Supplemental Fig. 9b). An increase in mean treatment current of 7.9A (1.4 ×) resulted in a 12 × increase in the thermal injury volume. This indicates that active cooling may be effective at reducing the temperature at the electrode-tissue interface, but may be insufficient to fully address the effect of Joule heating further from the electrode surface. As Joule heating (Q_{JH}) is a function of both current density (J) and electric field strength (E):

$$Q_{JH} = J \cdot E \left[\frac{W}{m^3}\right] \tag{8}$$

increases in current will result in a greater heating per unit volume. However the rate of heat transfer from the tissue to the coolant was likely independent of this experimental input. Therefore, treatments with greater average power delivery (e.g. approximately 65 W, Supplemental Fig. 9e) resulted in substantially larger regions of thermal injury surrounding the electrode than more conservative treatments (approximately 46 W, Fig. 3). When initial treatment currents were constrained perfusion at rates of 2, 4, and 8 mL/min were sufficient to mitigate the induction of thermal damage which became increasingly localized to the tip of the electrode. Taken in summation, these results indicate that active cooling of electrodes may not be sufficient for generically preventing the induction of thermal injury as treatment currents *in vivo* are dynamic and depend on tissue characteristics, applicator arrangement, applicator placement, and local temperatures. It is therefore important to implement some form of active feedback (e.g. temperature, current, power) management in these treatments to mitigate thermal injury.

The use of active temperature feedback by ETT from one, or multiple, locations is a potential solution to this challenge. As applicator cooling affects the temperature at the tissue electrode-tissue interface, it may be necessary to use temperature change, rather than absolute temperature, as the control signal. In this study, we demonstrate that dynamically adjusting the rate at which pulses are delivered is an effective method for achieving and maintaining a target temperature at the electrode-tissue interface. Without active cooling, the ETT algorithm was capable of maintaining temperatures of 30 °C (Supplemental Fig. 8), 40 °C, 50 °C, 60 °C, and 80 °C (Fig. 3), with the lower temperatures significantly reducing the extent of thermal injury at the expense of increased treatment times.

Interestingly, 50 °C treatments with active cooling resulted in larger thermal ablation zones than 50 °C treatments without cooling. The mean current values measured were not statistically different ($p = 0.3989$) in these treatments, however, the delivery rate (413 vs 87 μs/s) and thus average power delivered was much greater for the actively cooled treatments. It is likely that in this scenario, active perfusion was unable to remove enough energy to prevent thermal injury. It is possible that the temperature sensors were measuring an average temperature of both the cooled electrode surface and the warmer adjacent tissue resulting in a mischaracterization of the tissue temperature leading the algorithm to deliver energy at a higher rate than intended. To address this challenge, it may be necessary for future algorithms to implement a maximum power limit or use average power as a means for controlling the delivery rate. Alternatively, it may be necessary to record temperatures in locations where the thermal gradient is lower or at multiple locations. However, decreasing the temperature set point to 40 °C in conjunction with active cooling resulted in negligible thermal injury with substantially reduced treatment times compared to the 50 °C non-cooled treatments (54 vs. 343 s) indicating that selection of appropriate temperature set points may be sufficient for preventing thermal damage.

The R_{max} used in this study (500 μs/s) represented an extreme case which is approximately 5 $\times$ the rate typically used clinically. This R_{max} value was selected to examine the extent to which treatment times could be reduced, to overcome the highly efficient removal of heat at the electrode-tissue interface, and to test the limitations of the temperature control algorithm. While it may be feasible to use rates greater than 100 μs/s *in vivo*, caution should be exercised due to the potential to induce unintended thermal injury if temperature sensing is limited to the electrode-tissue interface. The results presented in Fig. 3 clearly demonstrate that thermal injury adjacent to the electrode is possible even if temperatures measured at the electrode are below 60 °C. In these scenarios there is likely an imbalance in the rate of Joule heating in the tissue surrounding the electrode and the rate of cooling due to electrode perfusion. As tissue is a relatively poor thermal conductor there is a natural limitation to the rate at which energy can be transferred through the tissue to the cooled electrode. This limitation is likely responsible for the observation (Fig. 4) that 5000 V non-cooled treatments at 50 °C resulted in similar thermal injury volumes to more rapid treatments with active cooling and a 40 °C set point. Future work will be necessary to determine the ideal rate of pulse delivery and control schemes which utilize true energy or power delivery calculations rather than energized-timing calculations may be necessary.

The localization of thermal injury towards the electrode tip may have been due to the internal geometry of the applicator which likely has a greater distance between the coolant and distal tip than the sidewalls of the electrode. This hypothesis is supported by numerical simulations (Fig. 2) which indicate that peak temperatures occur in proximity to the tip of the electrode. Alternatively, electrical corona may have formed at the sharp tip of the electrode resulting in an additional source of localized heating not present along the main body of the electrode. Corona were not observable through the opaque liver tissue, however, they appeared stochastically (Supplemental Fig. 4) in preliminary experiments conducted with the applicator placed 1–2 mm from a visible surface in muscle tissue.

Numerical simulations using lethal electric field data obtained from viable tissue indicate that the ablation created by purely electrical means (12.6 cm^3) would be greater than the maximum observed (2.6 cm^3) and predicted (2.2 cm^3) thermal injury volumes. Within the approximate 100 s duration of ETT treatments, simulated RFA treatments resulted in even smaller predicted thermal ablation volumes. This was likely due to the relatively high impedance load ($>$ 200 Ω) presented by the liver tissue in these experiments. This represents a potential advantage for high voltage pulsed electric field therapies as the outcomes are relatively independent of the load impedance assuming the generator is capable of supplying the requisite power. While outside the scope of this study, it is possible that these high voltage waveforms could be used to produce larger thermal ablations than RFA or MWA if treatment times were extended. In this scenario, temperature feedback would be remain necessary to prevent charring and desiccation at the electrode-tissue interface.

This study has several important limitations. Evaluation of thermal injury was conducted in an *ex vivo* non-perfused liver tissue model. While this is the accepted model for assessing thermal injury for radio frequency and microwave ablation[15] modalities, it does not enable the assessment of cell death due to irreversible electroporation which instead needed to be evaluated using computational models based on existing literature data.[17] Evaluation of IRE ablations requires either *in vivo* tissue or mechanical perfusion of viable organs. The treatments in this study were administered at room temperature (18–20 °C) which is substantially below physiological temperature (37 °C) and tissue conductivities may be higher *in vivo* leading to additional Joule heating. While the computationally derived tissue conductivity matched existing literature data, freeze/thaw cycling of commercially obtained tissue may have affected the observed thermal effects. *In vivo*, the uncontrolled treatment protocols administered in this study will likely result in peak temperatures more than 17 °C greater than those presented here due to feed forward effects of Joule heating. Therefore, it may not be possible to administer 5000 V, 200 μs/s treatments *in vivo* without exceeding 100 °C, unless an actively cooled electrode is used or a temperature control algorithm is implemented. Additionally, when implementing these active measures, treatment times *in vivo* may be greater than predicted here due to the elevated starting temperature. Finally, evaluating the effect of temperature regulation due to blood perfusion was not possible in *ex vivo* tissue. The presence of perfused micro- and macro-vasculature may affect the rate of tissue cooling *in vivo* favorably and the active temperature control algorithms implemented here should be capable of responding to real time variations in local perfusion due to the treatment.

Conclusion

In this study, a process for mitigating thermal injury in pulsed electric field therapies via an actively cooled electrode coupled with a dynamic feedback algorithm was presented. This combination enabled the rapid delivery of 5 kV irreversible electroporation protocols without the induction of thermal injury beyond the

electrode-tissue interface. The dynamic feedback algorithm was demonstrated as capable of maintaining tissue temperatures of 30, 40, 50, 60, and 80 °C independent of treatment parameters provided the tissue was heated sufficiently to reach the intended threshold. This work sets the foundation for *in vivo* studies using temperature sensors at the electrode-tissue interface and remote adjacent locations to prevent unwanted thermal injury to critical structures during pulsed electric field therapies.

ELECTRONIC SUPPLEMENTARY MATERIAL

The online version of this article (https://doi.org/10.1007/s10439-020-02524-x) contains supplementary material, which is available to authorized users.

ACKNOWLEDGMENTS

This work was supported in part by the provisioning of startup funding from the UNC/NCSU Joint Department of Biomedical Engineering.

CONFLICT OF INTEREST

MBS has provisional and accepted patents related to this work and receives royalties from AngioDynamics Inc. CCF and RAP have provisional patents related to this work.

REFERENCES

[1]Alonzo, M., A. Bos, S. Bennett, and H. Ferral. The Emprint™ ablation system with Thermosphere™ technology: one of the newer next-generation microwave ablation technologies. *Semin. Interv. Radiol.* 32:335–338, 2015.

[2]Arena, C. B., R. L. Mahajan, M. N. Rylander, and R. V. Davalos. Towards the development of latent heat storage electrodes for electroporation-based therapies. *Appl. Phys. Lett.* 101:083902, 2012.

[3]Bhonsle, S., M. Bonakdar, R. E. Neal, 2nd, C. Aardema, J. L. Robertson, J. Howarth, H. Kavnoudias, K. R. Thomson, S. N. Goldberg, and R. V. Davalos. Characterization of irreversible electroporation ablation with a validated perfused organ model. *J. Vasc. Interv. Radiol.* 27:1913–1922, 2016.

[4]Chen, S., G. Yin, W. Xu, W. Xi, and M. Zhang. Clinical research on advanced liver cancer treated with percutaneous RFA cool-tip electrode under ultrasound guidance. *J. Interv. Radiol.* 17:37–40, 2008.

[5]Diederich, C. J. Thermal ablation and high-temperature thermal therapy: overview of technology and clinical implementation. *Int. J. Hyperthermia* 21:745–753, 2005.

[6]Edelblute, C. M., J. Hornef, N. I. Burcus, T. Norman, S. J. Beebe, K. Schoenbach, R. Heller, C. Jiang, and S. Guo. Controllable moderate heating enhances the therapeutic efficacy of irreversible electroporation for pancreatic cancer. *Sci. Rep.* 7:11767, 2017.

[7]Faroja, M., M. Ahmed, L. Appelbaum, E. Ben-David, M. Moussa, J. Sosna, I. Nissenbaum, and S. N. Goldberg. Irreversible electroporation ablation: is all the damage nonthermal? *Radiology* 266:462–470, 2013.

[8]Feng, Y., J. TinsleyOden, and M. N. Rylander. A two-state cell damage model under hyperthermic conditions: theory and *in vitro* experiments. *J. Biomech. Eng.* 2008. https://doi.org/10.1115/1.2947320.

[9]Fesmire, C. C., R. A. Petrella, C. A. Fogle, D. Gerber, L. Xing, and M. B. Sano. Temperature dependence of high frequency irreversible electroporation evaluated in a 3d tumor model. *Ann. Biomed. Eng.* 2020. https://doi.org/10.1016/j.jvir.2019.05.009.

[10]Gabriel, C. Compilation of the dielectric properties of body tissues at rf and microwave frequencies. (DTIC Document, 1996).

[11]Garcia, P. A., J. H. Rossmeisl, Jr, T. L. Ellis, and R. V. Davalos. Nonthermal irreversible electroporation as a focal ablation treatment for brain cancer. *Tumors Central Nerv. Syst.* 12:171–182, 2014.

[12]Garcia, P. A., J. H. Rossmeisl, R. E. Neal, T. L. Ellis, and R. V. Davalos. A parametric study delineating irreversible electroporation from thermal damage based on a minimally invasive intracranial procedure. *Biomed. Eng. Online* 10:34, 2011.

[13]Golberg, A., and M. L. Yarmush. Nonthermal irreversible electroporation: fundamentals, applications, and challenges. *IEEE Trans. Biomed. Eng.* 60:707–714, 2013.

[14]Haemmerich, D., L. Chachati, A. S. Wright, D. M. Mahvi, F. T. Lee, and J. G. Webster. Hepatic radiofrequency ablation with internally cooled probes: effect of coolant temperature on lesion size. *IEEE Trans. Biomed. Eng.* 50:493–500, 2003.

[15]Hoffmann, R., H. Rempp, L. Erhard, G. Blumenstock, P. L. Pereira, C. D. Claussen, and S. Clasen. Comparison of four microwave ablation devices: an experimental study in ex vivo bovine liver. *Radiology* 268:89–97, 2013.

[16]Ierardi, A. M., A. Mangano, C. Floridi, G. Dionigi, A. Biondi, E. Duka, N. Lucchina, G. D. Lianos, and G. Carrafiello. a new system of microwave ablation at 2450 MHz: preliminary experience. *Upd. Surg.* 67:39–45, 2015.

[17]Kaufman, J. D., C. C. Fesmire, R. A. Petrella, C. A. Fogle, L. Xing, D. Gerber, and M. B. Sano. High-frequency irreversible electroporation using 5,000-V waveforms to create reproducible 2- and 4-cm ablation zones - a laboratory investigation using mechanically perfused liver. *J. Vasc. Interv. Radiol.* 2019. https://doi.org/10.1016/j.jvir.2019.05.009.

[18]Kourounis, G., P. PaulTabet, and D. Moris. Irreversible electroporation (Nanoknife® treatment) in the field of hepatobiliary surgery: current status and future perspectives. *J. BUON* 22:141–149, 2017.

[19]Kuang, M., M. D. Lu, X. Y. Xie, H. X. Xu, L. Q. Mo, G. J. Liu, Z. F. Xu, Y. L. Zheng, and J. Y. Liang. Liver cancer: increased microwave delivery to ablation zone with cooled-shaft antenna—experimental and clinical studies. *Radiology* 242:914–924, 2007.

[20]Liang, P., J. Yu, X.-L. Yu, X.-H. Wang, Q. Wei, S.-Y. Yu, H.-X. Li, H.-T. Sun, Z.-X. Zhang, and H.-C. Liu. Percutaneous cooled-tip microwave ablation under ultrasound guidance for primary liver cancer: a multicentre analysis of

1363 treatment-naive lesions in 1007 patients in China. *Gut* 61:1100–1101, 2012.
[21]Lundy, M., M. Garland-Kledzik, and P. Shen. Arterio-enteric fistula after irreversible electroporation. *Am. Surg.* 85:e55–e57, 2019.
[22]Martin, 2nd, R. C., D. Kwon, S. Chalikonda, M. Sellers, E. Kotz, C. Scoggins, K. M. McMasters, and K. Watkins. Treatment of 200 locally advanced (stage iii) pancreatic adenocarcinoma patients with irreversible electroporation: safety and efficacy. *Ann. Surg.* 262:486–494, 2015.
[23]Martin, R. C., K. McFarland, S. Ellis, and V. Velanovich. Irreversible electroporation in locally advanced pancreatic cancer: potential improved overall survival. *Ann. Surg. Oncol.* 20:443–449, 2013; discussion 492-484.
[24]Martin, R. C., E. Schwartz, J. Adams, I. Farah, and B. M. Derhake. Intra-operative anesthesia management in patients undergoing surgical irreversible electroporation of the pancreas, liver, kidney, and retroperitoneal tumors. *Anesthesiol. Pain Med.* 5:e22786, 2015.
[25]Miao, Y., Y. Ni, H. Bosmans, J. Yu, J. Vaninbroukx, S. Dymarkowski, H. Zhang, and G. Marchal. Radiofrequency ablation for eradication of renal tumor in a rabbit model by using a cooled-tip electrode technique. *Ann. Surg. Oncol.* 8:651–657, 2001.
[26]Moritz, A. R., and F. Henriques, Jr. Studies of thermal injury: II. The relative importance of time and surface temperature in the causation of cutaneous burns. *Am. J. Pathol.* 23:695, 1947.
[27]Narayanan, G., S. Bhatia, A. Echenique, R. Suthar, K. Barbery, and J. Yrizarry. Vessel patency post irreversible electroporation. *Cardiovasc. Intervent. Radiol.* 37:1523–1529, 2014.
[28]Ng, K., K. Chok, A. Chan, T. Cheung, T. Wong, J. Fung, J. Yuen, R. Poon, S. Fan, and C. Lo. Randomized Clinical Trial of Hepatic Resection Versus Radiofrequency Ablation for Early-Stage Hepatocellular Carcinoma. *Br. J. Surg.* 104:1775–1784, 2017.
[29]Ni, Y., Y. Miao, S. Mulier, J. Yu, A. Baert, and G. Marchal. A novel, ''cooled-wet'' electrode for radiofrequency ablation. *Eur. Radiol.* 10:852–854, 2000.
[30]Niessen, C., S. Thumann, L. Beyer, B. Pregler, J. Kramer, S. Lang, A. Teufel, E. Jung, C. Stroszczynski, and P. Wiggermann. Percutaneous irreversible electroporation: long-term survival analysis of 71 patients with inoperable malignant hepatic tumors. *Sci. Rep.* 7:43687, 2017.
[31]O'Brien, T. J., M. Bonakdar, S. Bhonsle, R. E. Neal, 2nd, C. H. Aardema, Jr, J. L. Robertson, S. N. Goldberg, and R. V. Davalos. Effects of internal electrode cooling on irreversible electroporation using a perfused organ model. *Int. J. Hyperther.* 35:44–55, 2018.
[32]Petrella, R. A., C. C. Fesmire, J. A. Kaufman, N. Topasna, and M. B. Sano. Algorithmically controlled electroporation: a technique for closed loop temperature regulated pulsed electric field cancer ablation. *IEEE Trans. Biomed. Eng.*, 2020 (in press).
[33]Philips, P., D. Hays, and R. C. Martin. Irreversible electroporation ablation (ire) of unresectable soft tissue tumors: learning curve evaluation in the first 150 patients treated. *PLoS ONE* 8:e76260, 2013.
[34]Sano, M. B., M. R. DeWitt, S. D. Teeter, and L. Xing. Optimization of a single insertion electrode array for the creation of clinically relevant ablations using high-frequency irreversible electroporation. *Comput. Biol. Med.* 95:107–117, 2018.
[35]Sano, M. B., R. E. Fan, G. L. Hwang, G. A. Sonn, and L. Xing. Production of spherical ablations using nonthermal irreversible electroporation: a laboratory investigation using a single electrode and grounding pad. *J. Vasc. Interv. Radiol.* 27:1432–1440, 2016.
[36]Sano, M. B., C. C. Fesmire, M. R. DeWitt, and L. Xing. Burst and continuous high frequency irreversible electroporation protocols evaluated in a 3d tumor model. *Phys. Med. Biol.* 63:135022, 2018.
[37]Shafiee, H., P. A. Garcia, and R. V. Davalos. A preliminary study to delineate irreversible electroporation from thermal damage using the arrhenius equation. *J. Biomech. Eng.* 131:074509, 2009.
[38]Wandel, A., E. Ben-David, B. S. Ulusoy, R. Neal, M. Faruja, I. Nissenbaum, S. Gourovich, and S. N. Goldberg. Optimizing Irreversible Electroporation Ablation with a Bipolar Electrode. *J. Vasc. Interv. Radiol.* 27:1441–1450, 2016.
[39]Wang, Y., Y. Sun, L. Feng, Y. Gao, X. Ni, and P. Liang. Internally cooled antenna for microwave ablation: results in ex vivo and in vivo porcine livers. *Eur. J. Radiol.* 67:357–361, 2008.
[40]Weaver, J. C., K. C. Smith, A. T. Esser, R. S. Son, and T. R. Gowrishankar. A brief overview of electroporation pulse strength-duration space: a region where additional intracellular effects are expected. *Bioelectrochemistry* 87:236–243, 2012.